RSC Advances

PAPER

View Article Online
View Journal | View Issue

Cite this: *RSC Adv.*, 2023, **13**, 8114

Palladium Schiff base complex-modified Cu(BDC-NH_2) metal–organic frameworks for C–N coupling†

Khadijeh Rabiei, *[a] Zahra Mohammadkhani,[a] Hassan Keypour [b] and Jamal Kouhdareh[b]

In this study, the synthesis of a novel functionalized metal–organic-framework (MOF) [Cu(BDC-NH_2)@Schiff-base-Pd(II)] catalyst *via* post-synthetic modification of Cu(BDC-NH_2) is reported. The targeted complex was prepared by chemically attaching *N*,*N*′-bis(5-formylpyrrol-2-ylmethyl) homopiperazine *via* a Schiff base reaction followed by complexation with Pd ions. Afterwards, the synthesized solid was applied as a very effective multifunctional catalyst in C–N coupling reactions. The synthesized compounds were identified by suitable techniques including N_2 isotherms, EDX spectroscopy, FT-IR spectroscopy, XRD, SEM, ICP-OES and TG-DTA. This nanocatalyst was used in C–N cross-coupling reactions, and it showed its usage in a diverse range of different functional groups with good efficiency. The reasons for introducing this catalyst system are its advantages such as considerably high selectivity, almost complete conversion of products, high yields, and convenient separation of catalysts and products. The results indicate that the highest efficiency of the product in the reaction was obtained in the shortest possible time with the use of [Cu(BDC-NH_2)@Schiff-base-Pd(II)] catalysts. Overall, the high catalytic activity of the [Cu(BDC-NH_2)@Schiff-base-Pd(II)] catalyst may be due to the obtained high surface area and the synergistic features created between Lewis acidic Cu nodes and Pd ions.

Received 14th February 2023
Accepted 24th February 2023

DOI: 10.1039/d3ra01020a

rsc.li/rsc-advances

1 Introduction

Metal–organic frameworks (MOFs) are a new class of mesoporous compounds, which due to their properties, have many applications in areas such as gas storage,[1,2] catalytic processes,[3–6] drug delivery,[7–9] encapsulation,[10] supercapacitance,[11] and heavy metal absorption.[12] Not only do MOFs possess higher levels of activation and stability than those of other classes of porous materials, but they are also capable of altering void morphology and size. This is an advantage in terms of improved separation and selectivity in applications.[13–15]

Post-synthetic modification of metal–organic frameworks is a common and practical approach to access MOF-based catalysts with the advantage of having multiple active sites, making this class of materials attractive to researchers.[16,17] Increasingly popular among designing and synthesizing new molecular scaffolds with unique structural and biological properties that enhance performance and selectivity is an interesting challenge. This MOF, a nanoporous compound, is stable under various conditions and can maintain its porosity as evidenced by its chemical and thermal robustness.[18–20]

In recent years, there have been numerous reports on the optimal performance of modified catalysts in MOF structures, including oxidation reactions, carbon–carbon coupling and reduction.[21,22] Some functional reports suggest MOFs as more popular candidates than other porous nanostructures.[23]

The Pd catalyst is an effective heterogeneous catalyst for carbon–carbon (C–C)[24] and carbon–nitrogen (C–N) coupling reactions,[25] such as the Heck reaction and Suzuki–Miyaura reaction,[26–30] reduction of nitroaromatic compounds[31–33] and oxidation of alcohol to aldehyde,[34] affording good to high yields. Our hopes for the approach of using metal–organic frameworks as catalyst supports provide a unique basis for the use of these mesoporous polymers in catalysis. A cross-coupling reaction is a transformation in which two fragments are joined together with the help of a metal catalyst. One of the most important reasons for using palladium-containing catalysts is their ability to carry out carbon–carbon and carbon–nitrogen cross-coupling reactions. *N*-Arylated compounds are available naturally and synthetically and have diverse applications in many fields.[35,36] This class of reactions is known as among the most important transformations in the synthesis of active medicinal substances.[37–46] Solid-phase organopalladium complexes in addition to high efficiency and activity have a very important

[a]*Department of Chemistry, Faculty of Science, Qom University of Technology, Qom, Iran. E-mail: rabiei@qut.ac.ir*

[b]*Department of Inorganic Chemistry, Faculty of Chemistry, Bu-Ali Sina University, Hamedan, 6517838683, Iran*

† Electronic supplementary information (ESI) available. See DOI: https://doi.org/10.1039/d3ra01020a

feature of selectivity, which helps in improving the synthesis of organic molecules. One of the types of important reactions is carbon–nitrogen coupling.[47,48]

In this research, a new palladium Schiff-base complex modified based on modified Cu(BDC-NH_2) metal–organic frameworks was designed and prepared. In the next step, after the synthesis of the Cu(BDC-NH_2) metal–organic framework, it was used as a support to make an organopalladium nanocatalyst. This nanocatalyst was used in the study of reaction for the assembly of 1,3-disubstituted pyrrolo[1,2-α]pyrazines, which obtained very good results with high efficiency and excellent stability of the nanocatalyst.

2 Experiments

2.1. Catalyst preparation

Cu(BDC-NH_2) was prepared according to the published method.[49–51] 2-Aminoterephthalic acid (NH_2-BDC) (1.087 g) and copper(II) nitrate (0.853 g) were added to a solution of dimethylformamide (DMF) (18 mL) and methanol (2 mL) transferred to a Teflon-lined stainless steel autoclave, stirred for 30 min, and then heated at 150 °C for 48 h. Next, Cu(BDC-NH_2) was obtained after washing and drying overnight.

In the next stage, a *N*,*N*′-bis(5-formylpyrrol-2-ylmethyl) homopiperazine (A) ligand was prepared by a general method,

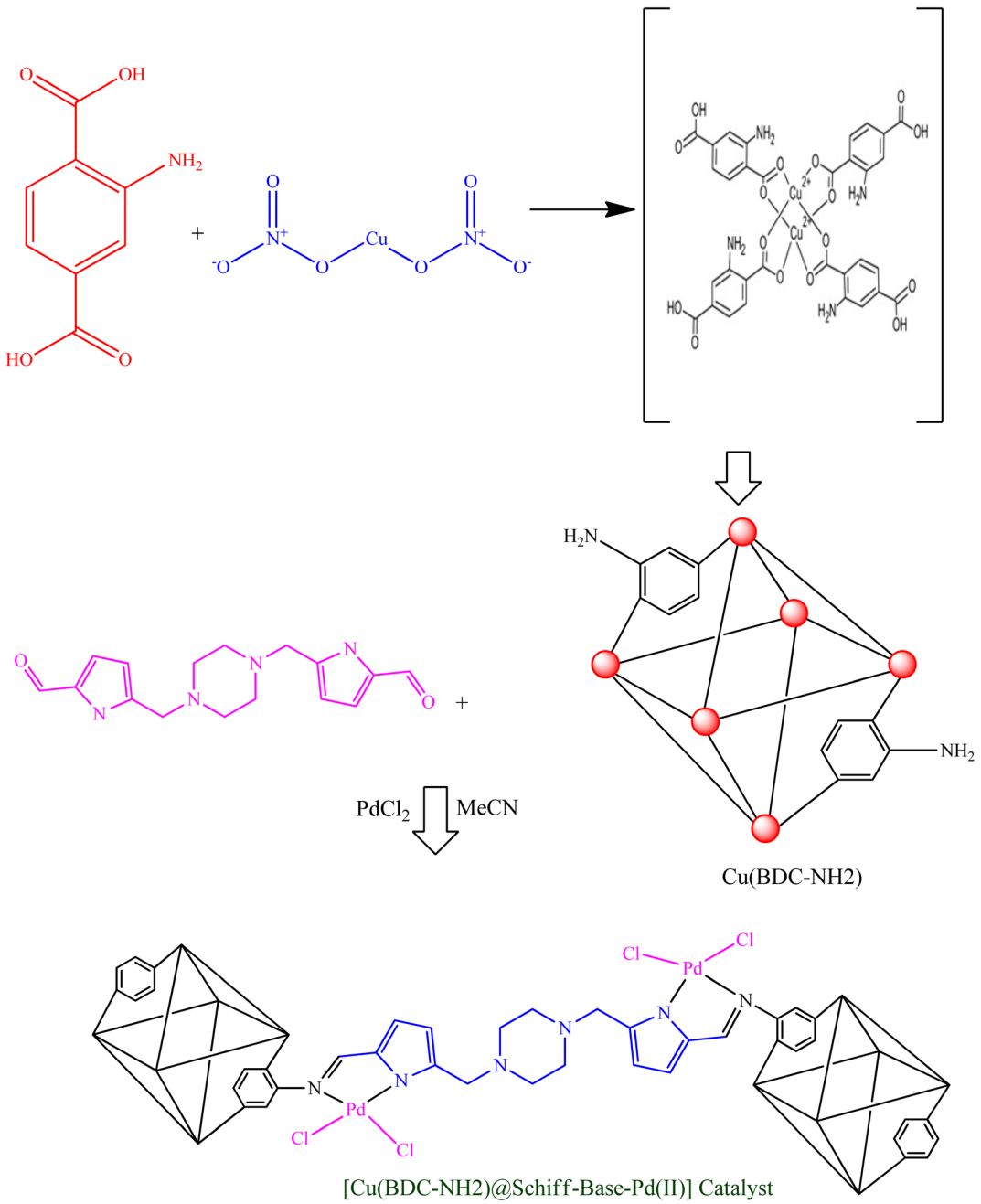

Scheme 1 Schematic of the synthetic procedure of the [Cu(BDC-NH_2)@Schiff-base-Pd(II)] catalyst.

as previously reported by Mani's group.[52] Then, the surface of Cu(BDC-NH_2) was functionalized with (A) to form Cu(BDC-NH_2)@Schiff-base: 1 g of prepared Cu(BDC-NH_2) was dispersed in dry ethanol (25 mL) by sonication for 30 min. Subsequently, a solution of ligand (3 mmol in dry ethanol (60 mL)) was added dropwise and the resulting solution was stirred for 24 h under reflux conditions. Afterward, the obtained Cu(BDC-NH_2)@Schiff-base was collected by centrifugation, washed with dry ethanol, and dried at 80 °C in an oven for 3 h.

Subsequently, Cu(BDC-NH_2)@Schiff-base (1.5 g) was dispersed in acetonitrile (30 mL) using an ultrasonic bath for 30 min. In the next step, a yellow solution of $PdCl_2$ (50 mg, 2.8 mmol) in 25 mL of acetonitrile was added to the dispersed Cu(BDC-NH_2)@Schiff-base and the mixture was stirred at room temperature for 24 h. Finally, Cu(BDC-NH_2)@Schiff-base-Pd(II) was separated by decantation and washed successively with acetonitrile, ethanol and acetone to remove the unattached substrates (Scheme 1).

2.2. Catalyst characterization

In this class of compounds, due to the large number and variety of functional groups, the number of peaks obtained in the spectrum is very high. This makes it impossible to properly interpret these graphs due to the overlap of the peaks (Fig. 1). The only help that these graphs provide is the connection of some peaks from the shift. Due to some limitations of detection techniques for the [Cu(BDC-NH_2)@Schiff-base-Pd(II)] catalyst, more accessible and desirable detection techniques should be used. The functional groups on the synthesized [Cu(BDC-NH_2)@Schiff-base-Pd(II)] solid were investigated by FTIR spectroscopy, which is shown in Fig. 1. The FTIR spectrum of Cu(BDC-NH_2) represented major stretching vibrations at 3400–3600 cm^{-1} (OH stretching and NH), 1717 cm^{-1} (C=O stretching), and 1690 cm^{-1} (C=N). All these peaks show blueshifts as Pd comes in the complex in [Cu(BDC-NH_2)@Schiff-base-Pd(II)], which reveals that the Pd complex is formed successfully.

Since most materials exhibit diffraction patterns specific to their structure, compounds can be identified using off-the-shelf databases or using information from similar articles. The purity of the sample and the composition of impurities present can be determined from the diffraction pattern, which can be used to determine and correct the lattice parameters of the crystal structure.[53]

The XRD patterns of the prepared Cu(BDC-NH_2), and [Cu(BDC-NH_2)@Schiff-base-Pd(II)] catalysts are shown in Fig. 2. The XRD pattern of the synthesized Cu(BDC-NH_2) shows characteristic peaks at 5–32°. The XRD pattern of the Cu(BDC-NH_2) represents a crystalline arrangement. Moreover, it demonstrates that the Cu(BDC-NH_2) center is maintained after conjugation. The XRD pattern of the prepared [Cu(BDC-NH_2)@Schiff-base-Pd(II)] catalyst shows the characteristic peaks of the Cu(BDC-NH_2) center at 2θ = 5–32°, and palladium characteristic peaks at 32°, 32.5°, 35° and 41°.[49] Hence, these observations prove the successful conjugation of *N*,*N*′-bis(5-formylpyrrol-2-ylmethyl) homopiperazine and complexation of palladium species on the Cu(BDC-NH_2) surface. The average particle size of the sample was estimated according to Scherer's formula, $D = 0.9\lambda/\beta\cos\theta$, where λ is the wavelength of the incident X-ray (0.154 nm), β is the full width of peak at half maxima and θ is Bragg's angle. The obtained value is 56 nm, consistent with the result measured from the SEM images[54] (Fig. 2).

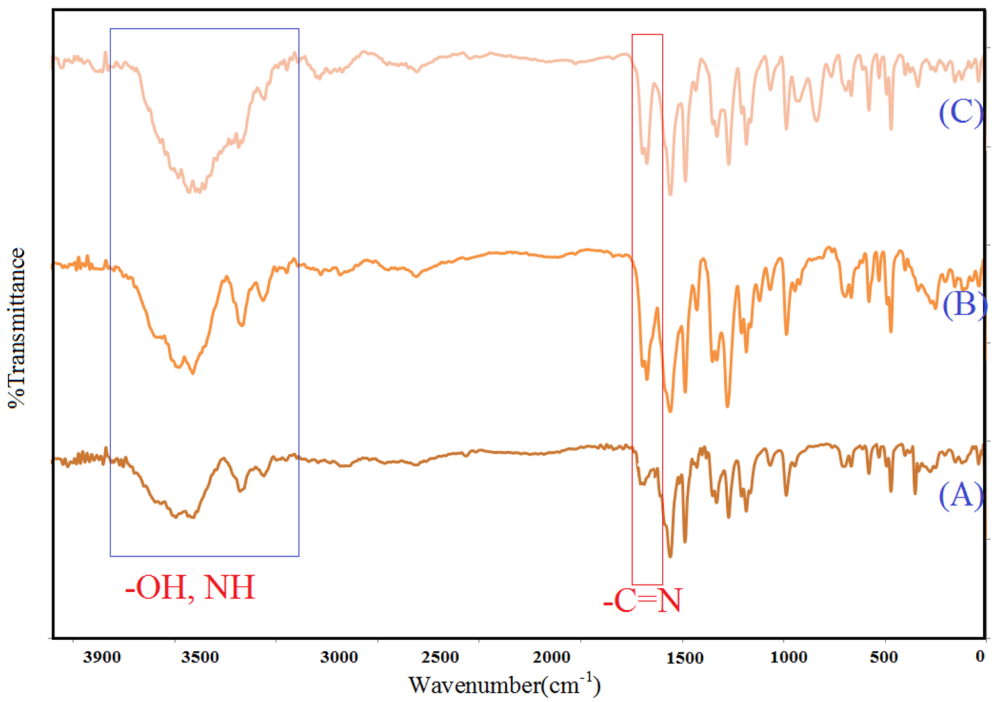

Fig. 1 FT-IR spectroscopy of Cu(BDC-NH_2) (A), Cu(BDC-NH_2) modified (B), and [Cu(BDC-NH_2)@Schiff-base-Pd(II)] catalyst (C).

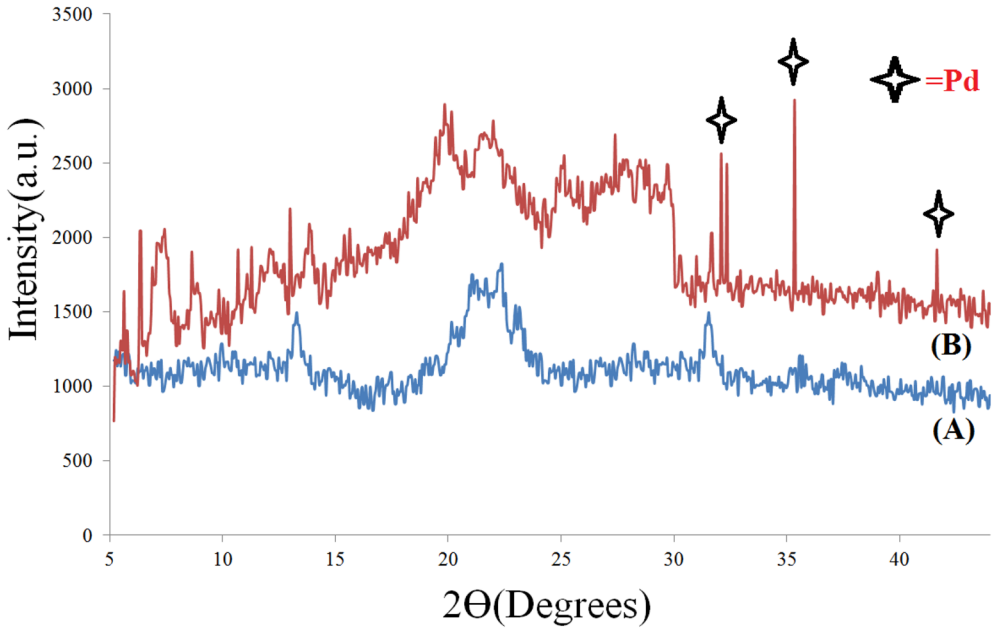

Fig. 2 X-ray diffraction (PXRD) pattern of Cu(BDC-NH_2) (A) and [Cu(BDC-NH_2)@Schiff-base-Pd(II)] catalyst (B).

Thermogravimetric analysis or thermal gravimetric analysis (TGA) is a method of thermal analysis in which the mass of a sample is measured over time as the temperature changes; by examining the curves of these patterns, the thermal stability of the compounds can be investigated.[55] Thermogravimetric analysis (TGA) spectra were used to investigate the thermal stability of the prepared Cu(BDC-NH_2) and [Cu(BDC-NH_2)@Schiff-base-Pd(II)] catalyst, as shown in Fig. 3. TGA shows weight loss up to 150 °C. This may be related to the evaporation of water molecules from the pores of the MOF and aromatic groups. After this weight loss, the weight remained unchanged up to 350 °C, indicating high thermal stability of the synthesized Cu(BDC-NH_2) and [Cu(BDC-NH_2)@Schiff-base-Pd(II)] catalyst.

To further characterize this palladium nanocatalyst sample, an extrapolated onset temperature can be calculated. This indicates the temperature at which weight loss begins. We use the extrapolated start temperature (T_0) for the nanocatalysts because it is a reproducible temperature calculation and is

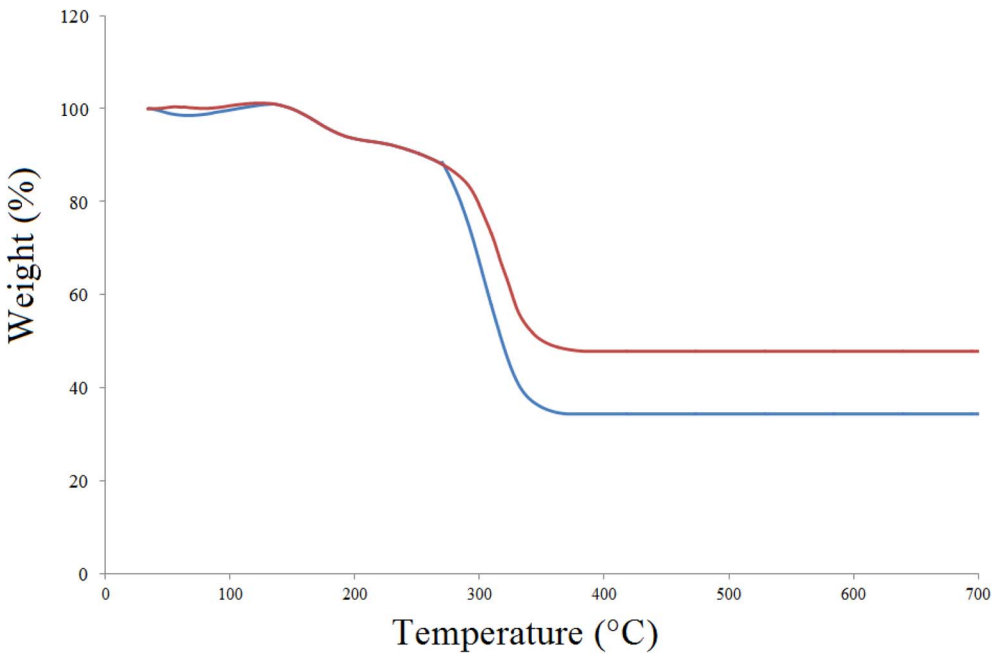

Fig. 3 Thermogravimetric analysis (TGA) for Cu(BDC-NH_2) (blue) and [Cu(BDC-NH_2)@Schiff-base-Pd(II)] catalyst (red).

specified for use with an extrapolated start temperature of 700 °C. This is the reason for the optimal thermal stability of this MOF-based synthetic nanocatalyst.

Scanning electron microscopy (SEM) is a technique that uses a focused beam of high-energy electrons to identify nanomaterials that produce distinct signals on the surface of solid samples (Fig. 4). Receiving these signals and processing the information obtained from them cause the electrons to interact with the sample, revealing information about the sample such as external morphology (texture), material orientation, crystal structure and chemical composition.[56] In these images, crystal structures and palladium nanoparticles with modified ligands on the surfaces of these organic–metal frameworks can be clearly seen.

An energy-dispersive X-ray spectroscopy (EDS, EDX, EDXS or XEDS) system is an accessory to electron microscopy equipment (scanning electron microscope (SEM) or transmission electron microscope (TEM) equipment) and the imaging capability of the microscope, which identifies the sample. The spectrum produced by EDX contains a spectrum analyzed for the peaks of the elements that make up the actual composition of the sample, giving the types of atoms available and the percentage of these atoms in the sample structure. The spectrum of the synthesized nanocatalyst shows the presence of elements C, N, O, Cu, Cl and Pd, which can be a sign of the success of the desired synthesis complex (Fig. 5). The appearance of Au* atoms in this spectrum is due to the kinetic of the sample during detection.[57]

We applied elemental mapping to complete the study on the elemental composition and distribution of the [Cu(BDC-NH_2)@Schiff-base-Pd(II)] catalyst (Fig. 6).Moreover, the elemental

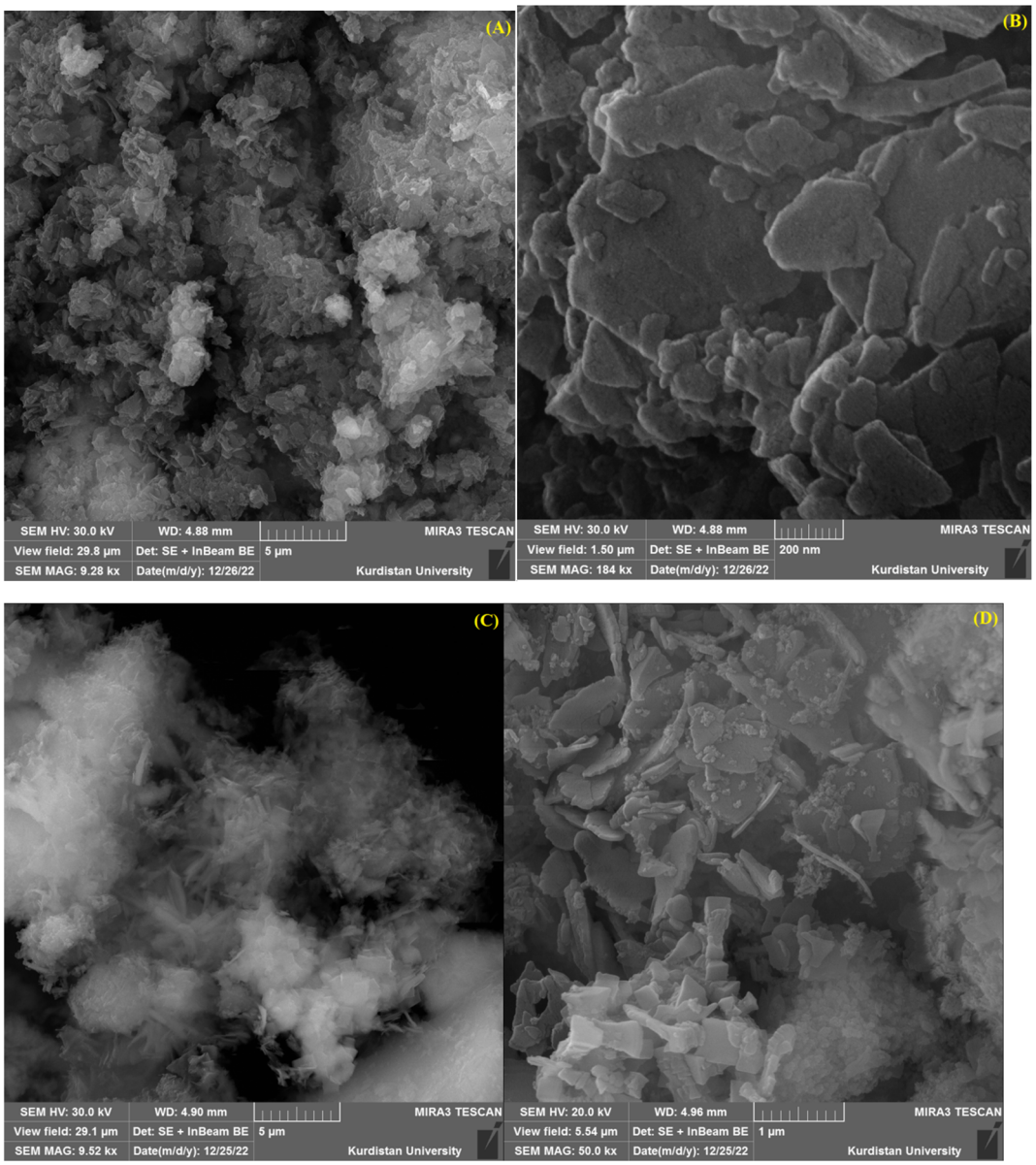

Fig. 4 Scanning electron microscopic (SEM) image of Cu(BDC-NH_2) (A and B) and [Cu(BDC-NH_2)@Schiff-base-Pd(II)] catalyst (C and D).

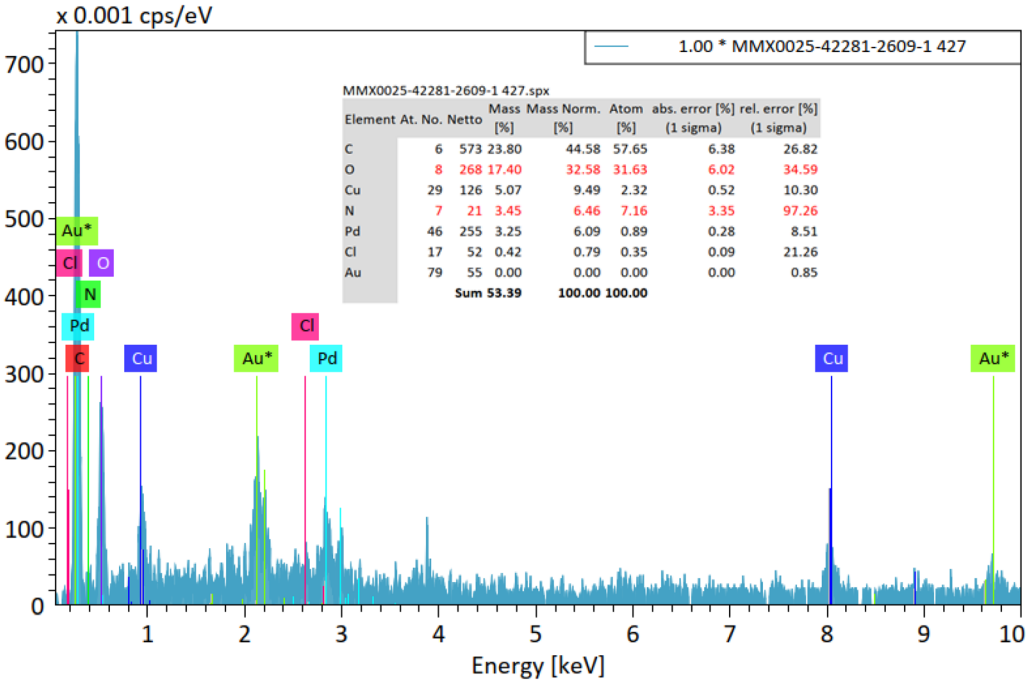

Fig. 5 Energy-dispersive X-ray (EDX) spectra of [Cu(BDC-NH_2)@Schiff-base-Pd(II)] catalyst.

mapping results are in good agreement with the EDX patterns. The elemental mapping image shows the well-uniform distribution of the exponential elements (Cu, N, O, C, Cl, and Pd) in the [Cu(BDC-NH_2)@Schiff base-Pd(II)] catalyst, confirming the synthesis of heterogenized [Cu(BDC-NH_2)@Schiff base Pd(II)] catalytic complexes. Furthermore, the distribution of Cu elements reveals the coordination of the resulting framework to the carboxylic acid groups and confirms the formation of the catalyst support. Furthermore, the distribution of C, N, O, Cl, and Pd species indicates that the final metal catalyst is uniformly coordinated to the Schiff base ligands and forms a Schiff base Pd shell on the catalyst support.

N_2 adsorption/desorption techniques were used to determine the surface structural parameters. The N_2 adsorption/desorption results are plotted in Fig. 7. The surface area obtained based on the BET isotherm is 136.16 $m^2\ g^{-1}$ and the total pore volume of the catalyst is 0.182 $cm^3\ g^{-1}$. The adsorption isotherm is of type III and the appearance of a hysteresis loop indicates the presence of mesopores in the sample.

2.3. Catalytic performance

2.3.1. General procedure for the synthesis of products. The amount of [Cu(BDC-NH_2)@Schiff base Pd(II)] catalyst (50 mg) and *p*-tolylboronic acid (1.5 mmol) with 1-(2-oxo-2-phenylethyl)-1*H*-pyrrole-2-added carbonitrile (0.6 mmol) in 5 mL of dimethylformamide to Table 1. After stirring for 24 hours at 70 °C, the mixture was cooled and filtered. The filtrate was diluted with ethyl acetate (30 mL) and washed with saturated brine. The aqueous layer was extracted with ethyl acetate (30 mL). The separated organic layer was dried over Na_2SO_4, concentrated *in vacuo* and the crude product was purified by column chromatography (silica gel) using petroleum ether/ethyl acetate (100 : 1, v/v) to A pure A product was obtained.

Based on the data obtained in Table 1, the C–N coupling reaction first occurred in the absence of catalyst at a temperature of 100 °C (entry 1) at which no product was formed. The optimal weight of the [Cu(BDC-NH_2)@Schiff base Pd(II)] catalyst (entry 6) is 50 mg. One of the parameters to optimize was the selection of suitable solvents for model reactions. According to the results of model reactions and optimization experiments, the highest efficiency of the C–N coupling reaction was obtained at a reaction temperature of 70 °C, a *N*,*N*-dimethylformamide (DMF) solvent volume of 5 mL, and a reaction time of 9 hours in an air atmosphere (Table 1, entry 14).

DMF will thermally decompose to give CO and dimethyl amine (presumably the method base is produced to deprotonate the ligands in MOF synthesis). This becomes more prominent at high temperatures. If you want to avoid formate formation, then you need to keep your reaction media scrupulously dry. We do this by using DMF from a solvent purification system and then using proper Schlenk technique.[58]

The [Cu(BDC-NH_2)@Schiff base Pd(II)] catalyst is used in the C–N coupling of *p*-tolylboronic acid and 1-(2-oxoethyl)-1*H*-pyrrole-2-carbonitrile carried out in DMF at 70 °C in an air atmosphere (Table 2, **3a–3h**). Compound 1-(2-oxoethyl)-1*H*-pyrrole-2-carbonitrile can be prepared by reacting hydrogen, hydrogen, transformed by different substitutions at the position of the donating group, or electron donating group. Although there is no logical and direct relationship with the efficiency of the reaction, it directly affected the rate and kinetics of the reaction. The reaction proceeded more slowly in the presence of the group.

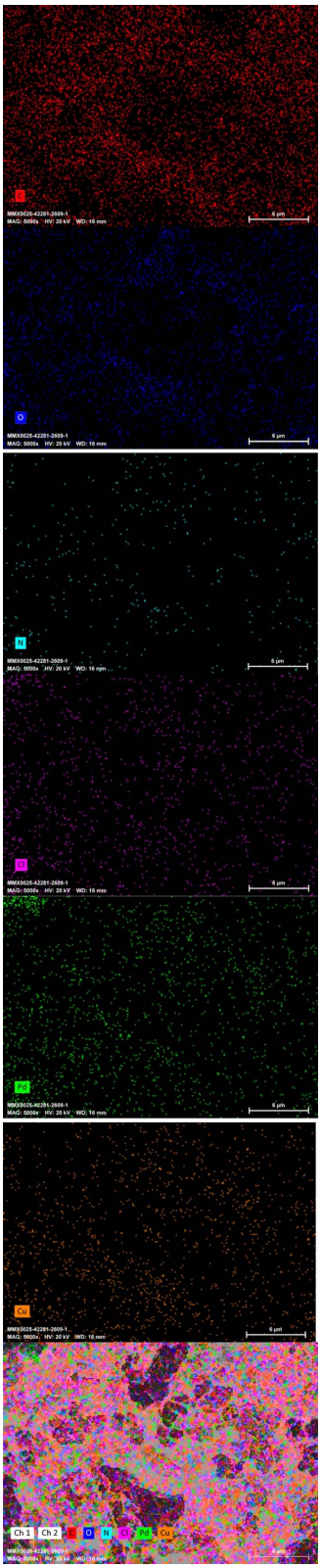

Fig. 6 X-ray mapping images of [Cu(BDC-NH_2)@Schiff-base-Pd(II)] catalyst.

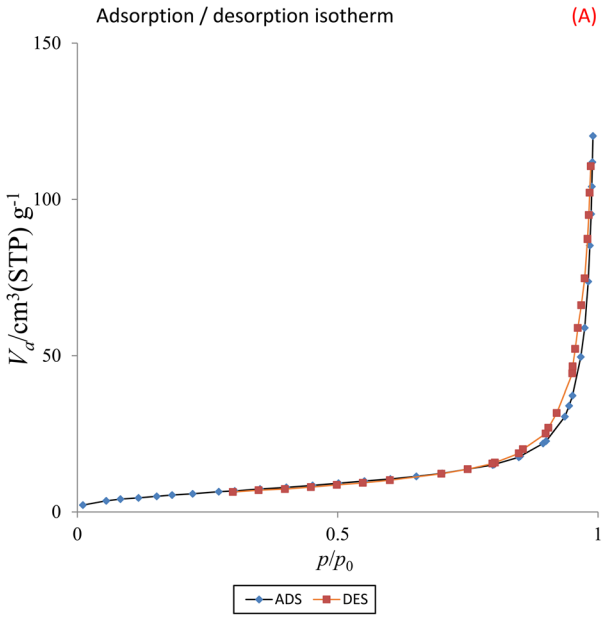

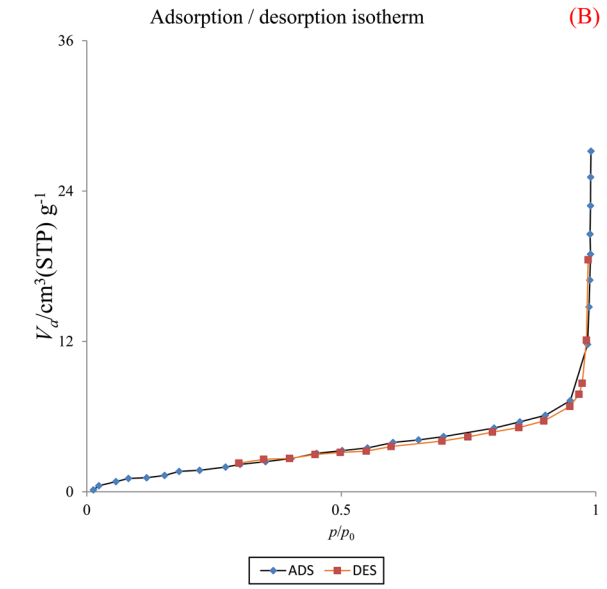

Sample	S_{BET} (m^2 g^{-1})	Total pure volume (cm^3 g^{-1})	Mean pore diameter (nm)
Cu(BDC-NH_2)	136.16	0.182	32.97
[Cu(BDC-NH_2)@Schiff-Base-Pd(II)] catalyst	8.34	0.0395	18.85

Fig. 7 N_2 adsorption–desorption isotherms of Cu(BDC-NH_2) (A) and [Cu(BDC-NH_2)@Schiff-base-Pd(II)] catalyst (B).

In Scheme 2, an acceptable mechanism for these reactions is proposed. In this mechanism, [Cu(BDC-NH_2)@Schiff base Pd(II)] reacts with aryl boric acid. Then, the cyano group forms the corresponding intermediate with the catalyst. Next, the aryl cyano group is condensed, and after that, the compound in question is synthesized by closing the ring and leaving the catalyst from the molecular structure.

The catalytic properties of the [Cu(BDC-NH_2)@Schiff base Pd(II)] catalyst were compared with those of other catalysts in

Table 1 Optimization of the C–N coupling reaction of *p*-tolylboronic acid with 1-(2-oxo-2-phenylethyl)-1*H*-pyrrole-2-carbonitrile using the [Cu(BDC-NH_2)@Schiff base Pd(II)] catalyst

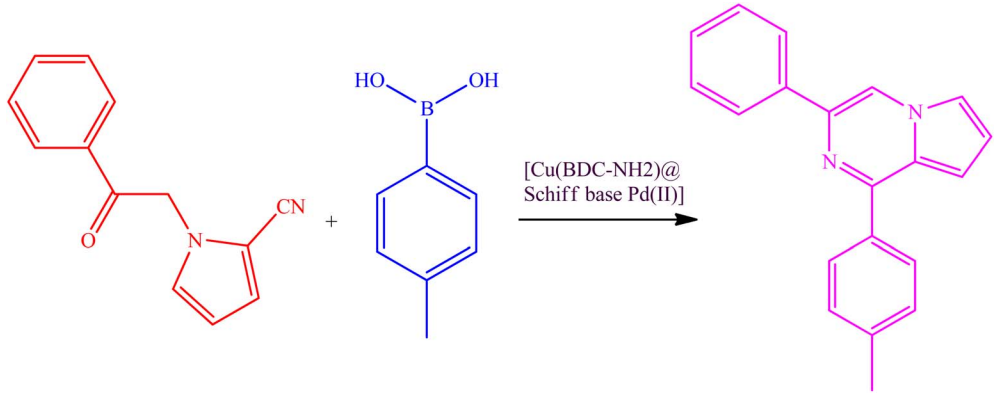

Entry	[Cu(BDC-NH_2)@Schiff base Pd(II)] catalyst (mg)	Solvent	Temperature (°C)	Yield[a] (%)
1	[Cu(BDC-NH_2)@Schiff base Pd(II)] catalyst (0)	MeCN	100	0.0
2	[Cu(BDC-NH_2)@Schiff base Pd(II)] catalyst (10)	MeCN	100	2.1
3	[Cu(BDC-NH_2)@Schiff base Pd(II)] catalyst (20)	MeCN	100	3.8
4	[Cu(BDC-NH_2)@Schiff base Pd(II)] catalyst (30)	MeCN	100	6.6
5	[Cu(BDC-NH_2)@Schiff base Pd(II)] catalyst (40)	MeCN	100	12.5
6	[Cu(BDC-NH_2)@Schiff base Pd(II)] catalyst (50)	MeCN	100	20.6
7	[Cu(BDC-NH_2)@Schiff base Pd(II)] catalyst (60)	MeCN	100	20.7
8	[Cu(BDC-NH_2)@Schiff base Pd(II)] catalyst (50)	Acetone	100	17.3
9	[Cu(BDC-NH_2)@Schiff base Pd(II)] catalyst (50)	Toluene	100	29.8
10	[Cu(BDC-NH_2)@Schiff base Pd(II)] catalyst (50)	Dioxane	100	43.2
11	[Cu(BDC-NH_2)@Schiff base Pd(II)] catalyst (50)	DMF	100	86.3
12	[Cu(BDC-NH_2)@Schiff base Pd(II)] catalyst (50)	DMF	90	86.5
13	[Cu(BDC-NH_2)@Schiff base Pd(II)] catalyst (50)	DMF	80	86.3
14	**[Cu(BDC-NH_2)@Schiff base Pd(II)] catalyst (50)**	**DMF**	**70**	**86.0**
15	[Cu(BDC-NH_2)@Schiff base Pd(II)] catalyst (50)	DMF	60	62.2

[a] Isolated yield.

Table 2 [Cu(BDC-NH_2)@Schiff base Pd(II)]-catalyzed *N*-arylation of 1-(2-oxoethyl)-1*H*-pyrrole-2-carbonitriles with *p*-tolylboronic acid[a]

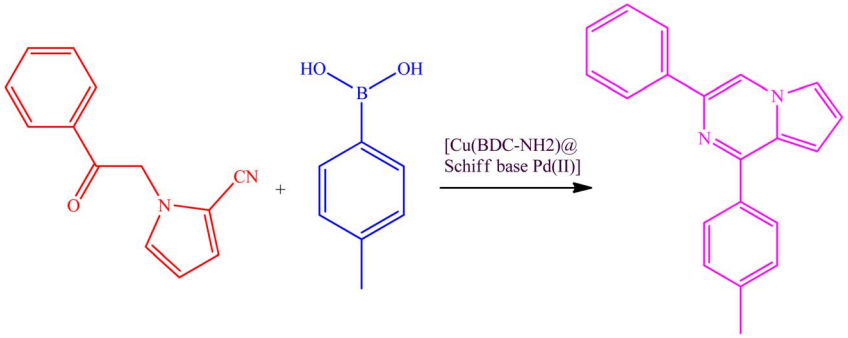

Entry	R1	R2	Product	Time (h)	Melting point (°C)	Appearance	Yield[b] (%)
1	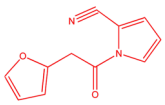	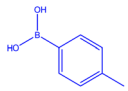	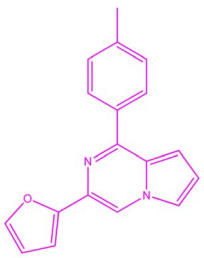 (3a)	18	129	White powder	66%
2	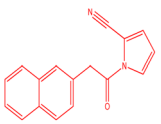	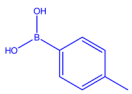	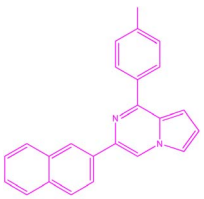 (3b)	22	118	White powder	64%
3	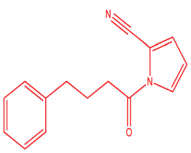	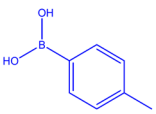	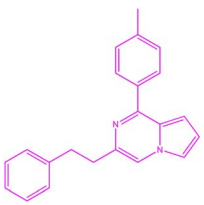 (3c)	16	190	Brown powder	65%
4	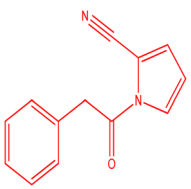	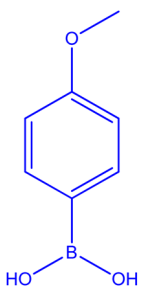	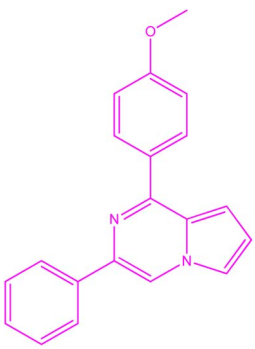 (3d)	23	139	Dark green powder	83%

Table 2 (*Contd.*)

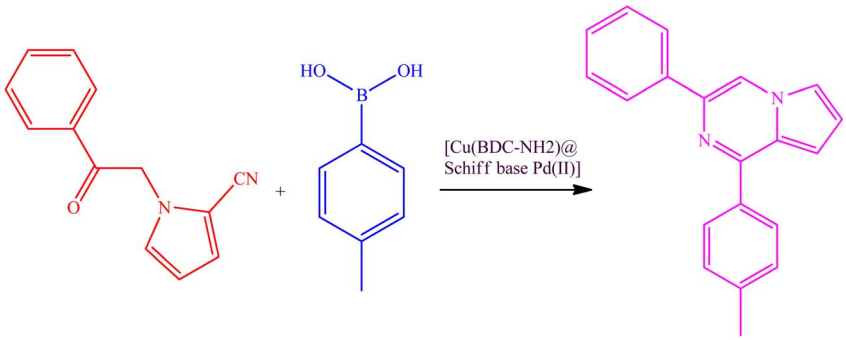

Entry	R1	R2	Product	Time (h)	Melting point (°C)	Appearance	Yield[b] (%)
5	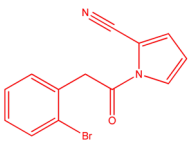	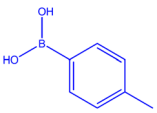	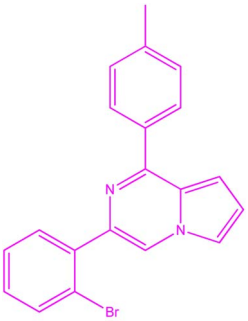 (3e)	16	100.5	White powder	71%
6	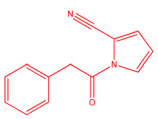	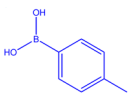	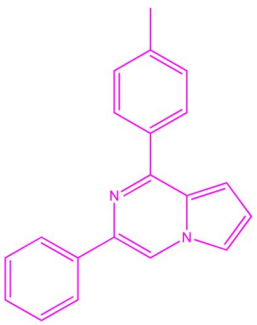 (3f)	17	127	White powder	85%
7	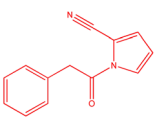	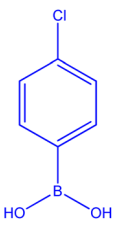	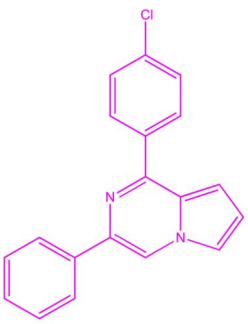 (3g)	22	170	Green powder	55%

Table 2 (*Contd.*)

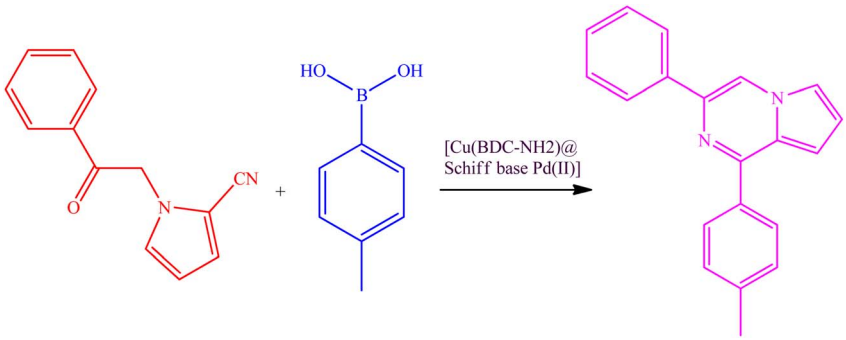

Entry	R1	R2	Product	Time (h)	Melting point (°C)	Appearance	Yield[b] (%)
8	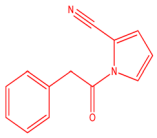	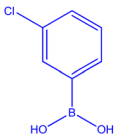	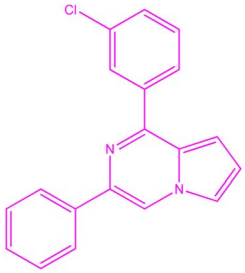 (3h)	19	138	Brown powder	42%

[a] Reactions were carried out in DMF at 70 °C for 24 h with the reaction components in the following ratio: *p*-tolylboronic acid (1.5 mmol), R1 in Table 2 derivatives (0.6 mmol), DMF (5 mL). [Cu(BDC-NH_2)@Schiff base Pd(II)] catalyst (50 mg). [b] Yield of the isolated product.

similar research articles. For this purpose, the results of these investigations are reported in Table 3. This catalyst had a higher efficiency than similar samples, and kinetically, the reactions occurred at a faster rate of progress. The new nanocatalyst is stable, non-toxic, economically viable, has simple synthesis steps, and is easily separated from the reaction.

Finally, it should be mentioned that the recycling and reuse of this nanocatalyst lead to a prospect for the synthesis of catalysts with a longer lifespan because the synthesis of this type of catalysts is expensive. It also requires special environmental conditions. After completing the reactions of the C–N coupling model, the catalyst can be easily separated from the reaction mixture by filtering and used in subsequent reactions by washing it several times with water and ethanol and drying it under vacuum (Fig. 8).

The recovery of the [Cu(BDC-NH_2)@Schiff base Pd(II)] catalyst in this study indicates a high-efficiency sequential application. The study of the XRD spectrum and scanning electron microscopic (SEM) images of the synthesized [Cu(BDC-NH_2)@Schiff base Pd(II)] catalyst after recovery shows the stability of this catalyst (Fig. 9). The Pd load in the material was found to be 7.54% and after recovery it was 7.33%, as estimated by the ICP-OES method.

After theoretical and experimental studies on these modified nanopolymers and proving their stability in reactions, it is necessary to use this class of compounds more than before.

2.3.2. General procedure for catalytic experiments

*3-(Furan-2-yl)-1-(p-tolyl)pyrrolo[1,2-a]pyrazine (**3a**).* ^{1}H NMR (500 MHz, chloroform-d) δ 8.22 (s, 1H), 7.95 (d, J = 8.0 Hz, 2H), 7.51 (m, 1H), 7.46 (m, 1H), 7.35–7.33 (m, 2H), 7.00 (d, J = 4.0, 1H), 6.96–6.94 (m, 1H), 6.52–6.51 (m, 1H), 6.28–6.26 (m, 1H), 2.44 (s, 3H).

^{13}C NMR (125 MHz, chloroform-d) δ 143.08, 141.92, 140.01, 131.06, 130.34, 129.31, 129.04, 128.98, 128.77, 116.20, 115.28, 111.90, 111.78, 107.29, 105.30, 21.60.

HRMS (ESI): m/z $[M + H]^+$ calcd for $C_{18}H_{15}N_2O$: 275.1179; found: 275.1205.

*3-(Naphthalen-2-yl)-1-(p-tolyl)pyrrolo[1,2-a]pyrazine (**3b**).* ^{1}H NMR (500 MHz, chloroform-d) δ 8.46 (s, 1H), 8.21 (m, 1H), 8.01–7.94 (m, 3H), 7.80–7.84 (m, 2H), 7.77–7.72 (m, 1H), 7.44–7.35 (m, 3H), 7.27 (d, J = 8.0 Hz, 2H), 6.88–6.89 (m, 1H), 6.80–6.81 (m, 1H), 2.37 (s, 3H).

^{13}C NMR (125 MHz, chloroform-d) δ 152.98, 139.92, 136.85, 135.94, 135.08, 133.81, 133.24, 129.33, 128.79, 128.56, 128.38, 127.76, 126.31, 126.23, 126.03, 124.98, 123.85, 115.90, 115.34, 115.34, 113.59, 104.62, 21.59.

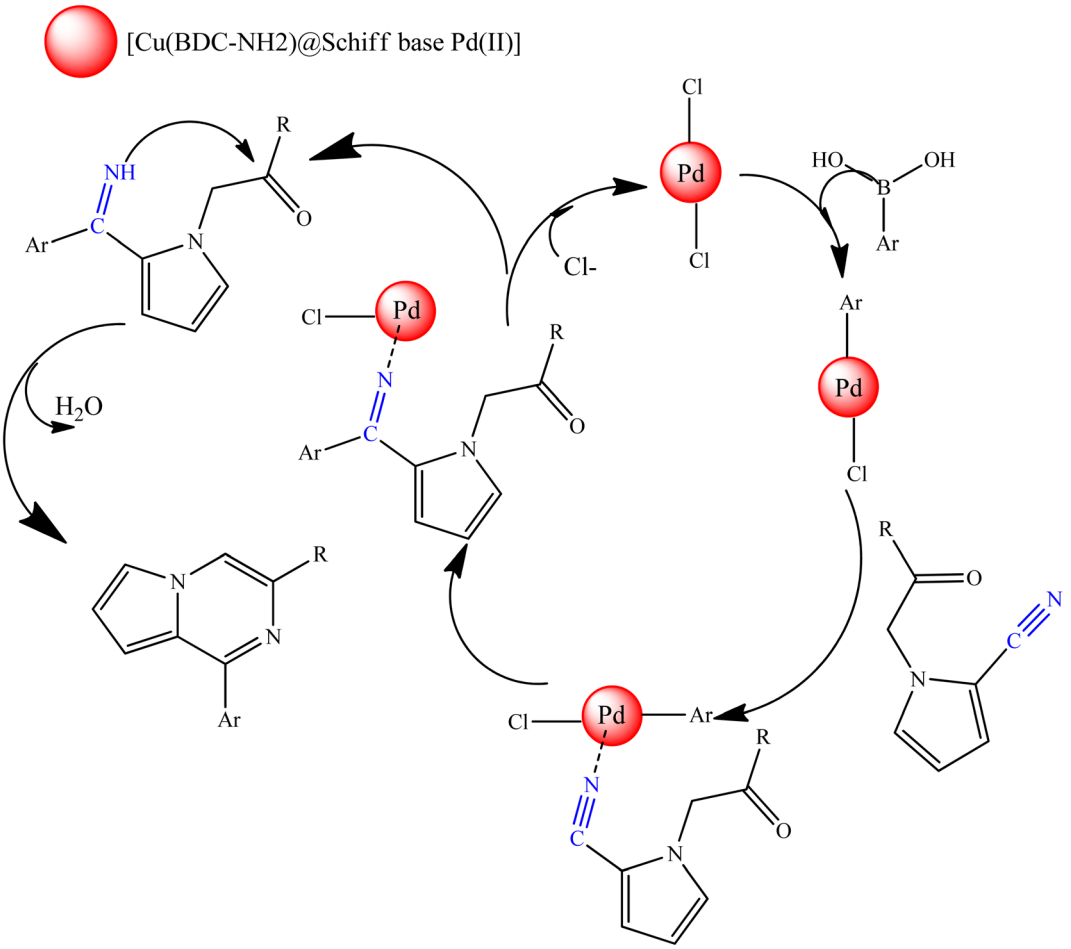

Scheme 2 Proposed mechanism for the *N*-arylation reaction using [Cu(BDC-NH_2)@Schiff base Pd(II)].

Table 3 Comparison of the effects of using different catalysts for the synthesis of products by C–N coupling

Entry	Catalyst	Product	Ref.
1	MCS-BAT-Cu(II)-catalyzed	1-Aryl-5-amino-1*H*-tetrazoles	59
2	Magnetic γ-Fe_2O_3@Cu-LDH	Quinolines	48
3	Pd/Cu-free co-catalyzed	Abemaciclib and Fedratinib	60
4	PNP-SSS	Buchwald–Hartwig C–N cross coupling	61
5	[Cu(BDC-NH_2)@Schiff base Pd(II)]catalyst	1-(2-Oxoethyl)-1*H*-pyrrole-2-carbonitriles with *p*-tolylboronic acid	This work

HRMS (ESI): *m*/*z* $[M + H]^+$ calcd for $C_{24}H_{19}N_2$: 335.1543; found: 335.1555.

*3-Phenethyl-1-(p-tolyl)pyrrolo[1,2-a]pyrazine (**3c**).* ^{1}H NMR (500 MHz, chloroform-d) δ 7.81–7.84 (m, 2H), 7.26–7.20 (m, 4H), 7.17–7.13 (m, 5H), 6.84–6.85 (m, 1H), 6.69–6.70 (m, 1H), 4.27 (s, 2H), 2.59 (s, 2H), 2.37 (s, 3H).

^{13}C NMR (125 MHz, chloroform-d) δ 151.32, 139.39, 136.00, 135.92, 133.77, 129.33, 129.10, 128.69, 127.84, 127.08, 127.02, 122.50, 114.82, 113.28, 104.81, 34.48, 21.55, 20.40.

HRMS (ESI): *m*/*z* $[M + H]^+$ calcd for $C_{22}H_{21}N_2$: 313.1966; found: 313.1945.

*1-(4-Methoxyphenyl)-3-phenylpyrrolo[1,2-a]pyrazine (**3d**).* ^{1}H NMR (500 MHz, chloroform-d) δ 8.18 (s, 1H), 8.09 (dd, *J* = 6.5, 2.0 Hz, 2H), 7.91 (m, 2H), 7.51 (dd, *J* = 2.5, 1.5 Hz, 1H), 7.27 (m, 3H), 7.06 (dd, *J* = 6.5, 2.0 Hz, 2H), 6.95 (m, 1H), 6.89 (dd, *J* = 4.5, 2.5 1H), 3.90 (s, 3H).

^{13}C NMR (125 MHz, chloroform-d) δ 159.87, 151.26, 136.76, 135.89, 130.20, 129.08, 127.64, 126.82, 124.97, 124.87, 114.64, 114.08, 112.83, 111.91, 103.28, 54.38.

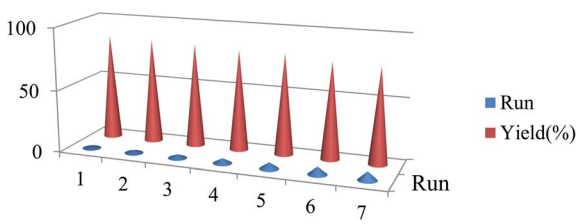

Fig. 8 Recycling performance of the [Cu(BDC-NH_2)@Schiff base Pd(II)] catalyst in the *N*-acrylate core of *p*-tolylboronic acid with derivatives R1 provided in Table 2 (entries 1–7).

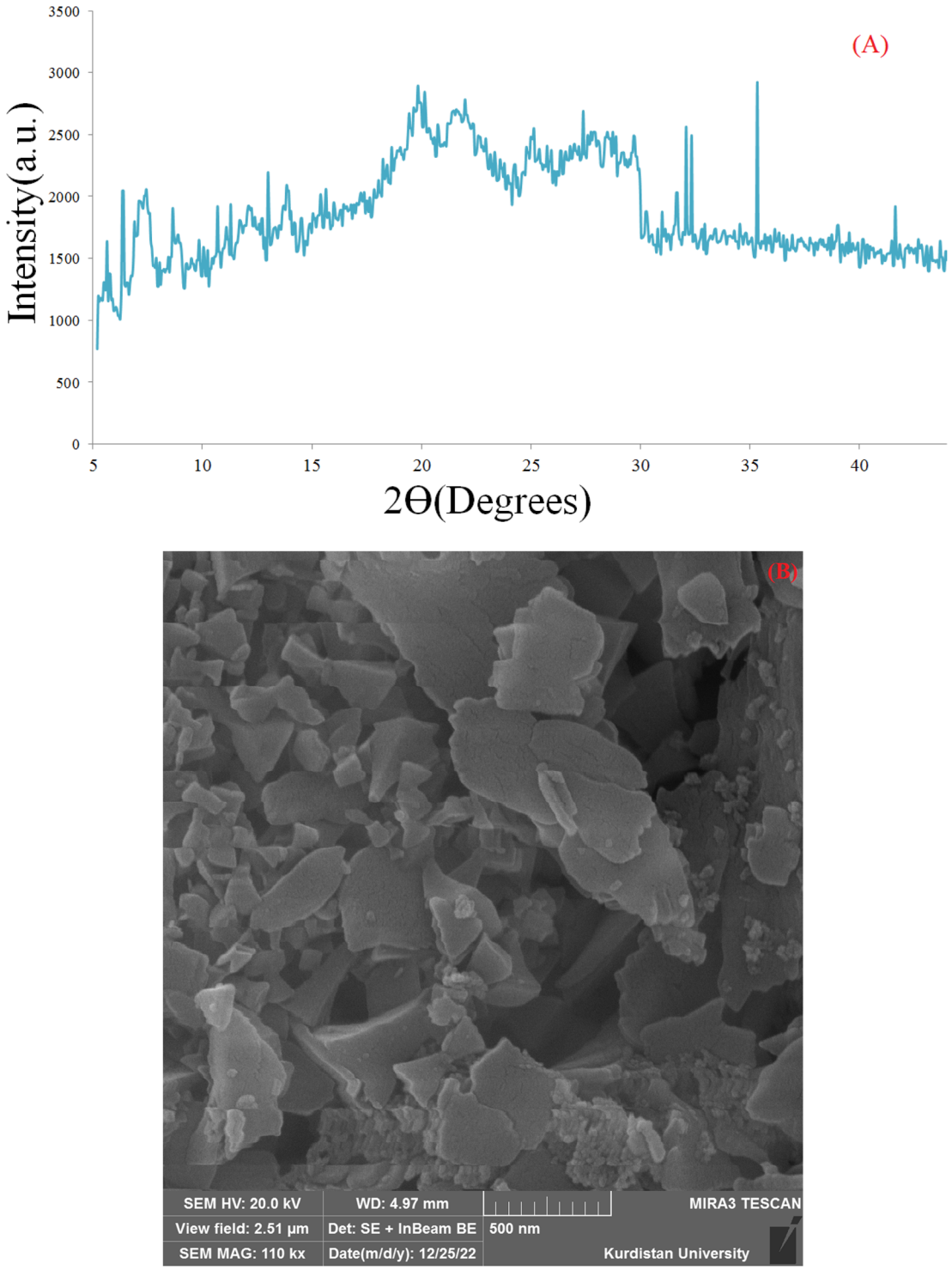

Fig. 9 XRD spectrum of the [Cu(BDC-NH_2)@Schiff base Pd(II)] catalyst after recovery (A) and scanning electron microscopic (SEM) image of the [Cu(BDC-NH_2)@Schiff base Pd(II)] catalyst after recovery (B).

HRMS (ESI): *m*/*z* $[M + H]^+$ calcd for $C_{20}H_{17}N_2O$: 301.1335; found: 301.1323.

*3-(2-Bromophenyl)-1-(p-tolyl)pyrrolo[1,2-a]pyrazine (**3e**).* ^1H NMR (500 MHz, chloroform-d) δ 8.11 (s, 1H), 7.98 (d, $J = 8.0$ Hz, 2H), 7.69–7.71 (m, 2H), 7.53–7.54 (m, 1H), 7.39–7.42 (m, 1H), 7.32–7.33 (m, 1H), 7.21–7.23 (m, 2H), 7.00 (m, 1H), 6.94–6.95 (m, 1H), 2.44 (s, 3H).

^{13}C NMR (125 MHz, chloroform-d) δ 152.95, 139.86, 137.23, 135.74, 133.61, 132.04, 129.47, 129.33, 128.74, 127.65, 127.28, 124.01, 122.80, 117.10, 115.86, 115.50, 104.64, 21.60.

HRMS (ESI): *m*/*z* $[M + H]^+$ calcd for $C_{20}H_{15}BrN_2$: 363.0491; found: 363.0499.

*3-Phenyl-1-(p-tolyl)pyrrolo[1,2-a]pyrazine (**3f**).* ^1H NMR (500 MHz, chloroform-d) δ 8.11 (s, 1H), 8.02 (dd, $J = 8.0$, 1.5 Hz, 2H),

7.83 (d, $J = 8.0$, 2H), 7.47–7.41 (m, 4H), 7.18 (d, $J = 8.0$ Hz, 2H), 6.87 (dd, $J = 4.5$, 1.5 Hz, 1H), 6.81 (dd, $J = 4.0$, 2.5 Hz, 1H), 2.32 (s, 3H).

^{13}C NMR (125 MHz, chloroform-d) δ 151.72, 138.70, 136.72, 135.92, 134.77, 128.13, 127.63, 127.58, 126.82, 125.07, 124.87, 114.62, 114.12, 112.10, 103.32, 20.42.

HRMS (ESI): m/z $[M + H]^+$ calcd for $C_{20}H_{17}N_2$: 285.1386; found: 285.1376.

*1-(4-Chlorophenyl)-3-phenylpyrrolo[1,2-a]pyrazine (**3g**).* Green solid; yield: 136.1 mg (49%); mp 169.8–170.1 °C.

^{1}H NMR (500 MHz, chloroform-d) δ 8.14 (s, 1H), 7.98 (t, $J =$ 2.0 Hz, 1H), 7.97 (t, $J = 2.0$ Hz, 1H), 7.94–7.89 (dd, $J = 8.0$, 1.0 Hz, 2H), 7.47–7.45 (m, 1H), 7.42 (t, $J = 2.0$ Hz, 1H), 7.38 (dd, $J = 6.0$, 2.0 Hz, 2H), 7.30–7.26 (m, 1H), 6.85–6.83 (m, 2H).

^{13}C NMR (125 MHz, chloroform-d) δ 151.65, 137.56, 137.09, 137.01, 134.69, 130.13, 130.01, 129.59, 128.73, 128.65, 127.91, 115.52, 113.49, 103.28.

HRMS (ESI): m/z $[M + H]^+$ calcd for $C_{19}H_{14}ClN_2$: 305.0840; found: 305.0854.

*1-(3-Chlorophenyl)-3-phenylpyrrolo[1,2-a]pyrazine (**3h**).* ^{1}H NMR (500 MHz, chloroform-d) δ 8.24 (s, 1H), 8.06 (dd, $J = 6.5$, 1.5 Hz, 2H), 8.00 (dd, $J = 4.5$, 1.5 Hz, 2H), 7.56–7.45 (m, 5H), 7.39–7.36 (m, 1H), 6.93–6.92 (m, 2H).

^{13}C NMR (125 MHz, chloroform-d) δ 151.55, 137.50, 137.04, 137.01, 135.69, 130.10, 130.02, 129.59, 128.73, 128.05, 125.91, 125.87, 115.52, 113.49, 104.22.

HRMS (ESI): m/z $[M + H]^+$ calcd for $C_{19}H_{14}ClN_2$: 305.0840; found: 305.0864.

3 Conclusion

The [Cu(BDC-NH_2)@Schiff base Pd(II)] nanocatalyst was synthesized as a novel nanocomposite *via* a two-step post-synthetic modification reaction of Cu(BDC-NH_2) with *N*,*N*′-bis(5-formylpyrrol-2-ylmethyl) homopiperazine followed by Pd ion immobilization.

The characterization of the [Cu(BDC-NH_2)@Schiff base Pd(II)] catalyst was done by ICP-OES, TG-DTA, FT-IR spectroscopy, EDX spectroscopy, XRD, and N_2 isotherms. Other contributors are the cooperative effect between the amine sites and the large surface area, and the high porosity of MOFs. In addition, [Cu(BDC-NH_2)@Schiff base Pd(II)] was found to be a multifunctional MOF with robustness and stability under the reaction conditions. Accordingly, it can be reused up to seven times without losing its catalytic activity and structural integrity. The other benefits of the proposed mesoporous catalyst include high yields, facile separation of the catalyst from the mixture, and clean reaction profile. This research portrays a bright future of using porous MOFs and their functionalized analogs as multifunctional catalysts.

Conflicts of interest

The authors declare that they have no known competing financial interests or personal relationships that could have appeared to influence the work reported in this paper.

Acknowledgements

Funding of our research from the Qom University of Technology is gratefully acknowledged.

References

1 H. Daglar, *et al.*, Effect of metal–organic framework (MOF) database selection on the assessment of gas storage and separation potentials of MOFs, *Angew. Chem., Int. Ed.*, 2021, **60**(14), 7828–7837.
2 D. Alezi, *et al.*, MOF crystal chemistry paving the way to gas storage needs: aluminum-based soc-MOF for CH_4, O_2, and CO_2 storage, *J. Am. Chem. Soc.*, 2015, **137**(41), 13308–13318.
3 J. Liu, *et al.*, MOF-enabled confinement and related effects for chemical catalyst presentation and utilization, *Chem. Soc. Rev.*, 2022, **51**, 1045–1097.
4 F. Ghobakhloo, *et al.*, Copper (II) Schiff-Base Complex Modified UiO-66-NH_2 (Zr) Metal–Organic Framework Catalysts for Knoevenagel Condensation–Michael Addition–Cyclization Reactions, *Inorg. Chem.*, 2022, **61**(12), 4825–4841.
5 J. Kouhdareh, H. Keypour and S. Alavinia, Anchorage of Pd into Modified Isoreticular Metal–Organic Framework-3 as a Heterogeneous Catalyst for Mizoroki–Heck Crosscoupling Reactions, *Acta Chem. Malaysia*, 2022, **6**(1), 35–42.
6 H. Keypour, *et al.*, Post-synthetic modification of dual-porous UMCM-1-NH_2 with palladacycle complex as an effective heterogeneous catalyst in Suzuki and Heck coupling reactions, *J. Organomet. Chem.*, 2023, 122646.
7 J. Cao, X. Li and H. Tian, Metal-organic framework (MOF)-based drug delivery, *Curr. Med. Chem.*, 2020, **27**(35), 5949–5969.
8 S. Mallakpour, E. Nikkhoo and C. M. Hussain, Application of MOF materials as drug delivery systems for cancer therapy and dermal treatment, *Coord. Chem. Rev.*, 2022, **451**, 214262.
9 H. Keypour, J. Kouhdareh, S. Alavinia and A. Maryamabadi, Application of $Co_3(BTC)_2 \cdot 12H_2O$ as a Metal-Organic Framework in Controlled Uptake-Release of Oxaliplatin, *Acta Chem. Malaysia*, 2022, **6**(2), 100–105.
10 N. Liédana, *et al.*, The template role of caffeine in its one-step encapsulation in MOF NH 2-MIL-88B (Fe), *J. Mater. Chem. B*, 2014, **2**(9), 1144–1151.
11 S. Wu, *et al.*, A review of performance optimization of MOF-derived metal oxide as electrode materials for supercapacitors, *Int. J. Energy Res.*, 2019, **43**(2), 697–716.
12 E. Tahmasebi, *et al.*, Application of mechanosynthesized azine-decorated zinc (II) metal–organic frameworks for highly efficient removal and extraction of some heavy-metal ions from aqueous samples: a comparative study, *Inorg. Chem.*, 2015, **54**(2), 425–433.
13 J.-R. Li, R. J. Kuppler and H.-C. Zhou, Selective gas adsorption and separation in metal–organic frameworks, *Chem. Soc. Rev.*, 2009, **38**(5), 1477–1504.
14 A. U. Czaja, N. Trukhan and U. Müller, Industrial applications of metal–organic frameworks, *Chem. Soc. Rev.*, 2009, **38**(5), 1284–1293.

15 W. G. Cui, T. L. Hu and X. H. Bu, Metal–organic framework materials for the separation and purification of light hydrocarbons, *Adv. Mater.*, 2020, **32**(3), 1806445.
16 Z. Yin, *et al.*, Recent advances in post-synthetic modification of metal–organic frameworks: New types and tandem reactions, *Coord. Chem. Rev.*, 2019, **378**, 500–512.
17 Q. Yu, *et al.*, Advances in luminescent metal-organic framework sensors based on post-synthetic modification, *TrAC, Trends Anal. Chem.*, 2020, **129**, 115939.
18 K. Akhbari and A. Morsali, Modulating methane storage in anionic nano-porous MOF materials *via* post-synthetic cation exchange process, *Dalton Trans.*, 2013, **42**(14), 4786–4789.
19 F. Marpaung, *et al.*, Metal–organic framework (MOF)-derived nanoporous carbon materials, *Chem.–Asian J.*, 2019, **14**(9), 1331–1343.
20 M. Kim, *et al.*, MOF-derived nanoporous carbons with diverse tunable nanoarchitectures, *Nat. Protoc.*, 2022, 1–42.
21 C. Zhu, *et al.*, Highly efficient nonprecious metal catalysts towards oxygen reduction reaction based on three-dimensional porous carbon nanostructures, *Chem. Soc. Rev.*, 2016, **45**(3), 517–531.
22 P. Gotico, Z. Halime and A. Aukauloo, Recent advances in metalloporphyrin-based catalyst design towards carbon dioxide reduction: from bio-inspired second coordination sphere modifications to hierarchical architectures, *Dalton Trans.*, 2020, **49**(8), 2381–2396.
23 W. Xia, *et al.*, Metal–organic frameworks and their derived nanostructures for electrochemical energy storage and conversion, *Energy Environ. Sci.*, 2015, **8**(7), 1837–1866.
24 J. Kouhdareh, *et al.*, Pd (II)-immobilized on a novel covalent imine framework (COF-BASU1) as an efficient catalyst for asymmetric Suzuki coupling, *J. Mol. Struct.*, 2023, **1273**, 134286.
25 N. M. Camasso and M. S. Sanford, Design, synthesis, and carbon-heteroatom coupling reactions of organometallic nickel (IV) complexes, *Science*, 2015, **347**(6227), 1218–1220.
26 M. Aghayee, *et al.*, Synthesis and characterization of a novel magnetic nano-palladium Schiff base complex: application in cross-coupling reactions, *Appl. Organomet. Chem.*, 2016, **30**(8), 612–618.
27 H. Keypour, *et al.*, Synthesis of magnetically recyclable Fe_3O_4@[(EtO) 3Si–L1H]/Pd (II) nanocatalyst and application in Suzuki and Heck coupling reactions, *Appl. Organomet. Chem.*, 2017, **31**(2), e3558.
28 D. Habibi, *et al.*, A green and facile approach for the synthesis of N-monosubstituted ureas in water: Pd catalyzed reaction of arylcyanamides (an unexpected behavior of electron withdrawing groups), *Polyhedron*, 2018, **151**, 520–529.
29 M. Balali, *et al.*, Palladium Supported on Schiff Base Functionalized Magnetite Nanoparticles as an Efficient Catalyst for Coupling Reactions, *Inorg. Chem. Res.*, 2021, **5**(1), 82–93.
30 H. Keypour, J. Kouhdareh, S. Alavinia and M. t. Rezaei, Synthesis of Magnetic Nano Catalyst Using Dopamine Functionalized Magnetic Nano Particles and Investigation of Its Properties in Mizoroki–Heck Cross-Coupling Reactions, *Acta Chem. Malaysia*, 2023, **7**(1), 16–22.
31 H. Keypour and M. Noroozi, Hydrogenation of benzene in gasoline fuel over nanoparticles (Ni, Pt, Pd, Ru and Rh) supported fullerene: Comparison study, *J. Appl. Chem.*, 2016, **10**, 31–42.
32 H. Keypour, Application of Response Surface Methodology for Catalytic Hydrogenation of Nitrobenzene to Aniline Using Ruthenium Supported Fullerene, *Nanocatalyst*, 2015, **34**, 21–32.
33 J. Kouhdareh, *et al.*, Immobilization of Ag and Pd over a novel amide based covalent organic framework (COF-BASU2) as a heterogeneous reusable catalyst to reduce nitroarenes, *Inorg. Chim. Acta*, 2023, **545**, 121251.
34 B. Karimi, *et al.*, Highly efficient aerobic oxidation of alcohols using a recoverable catalyst: the role of mesoporous channels of SBA-15 in stabilizing palladium nanoparticles, *Angew. Chem., Int. Ed.*, 2006, **45**(29), 4776–4779.
35 D. Enders, O. Niemeier and A. Henseler, Organocatalysis by N-heterocyclic carbenes, *Chem. Rev.*, 2007, **107**(12), 5606–5655.
36 S. D. Roughley and A. M. Jordan, The medicinal chemist's toolbox: an analysis of reactions used in the pursuit of drug candidates, *J. Med. Chem.*, 2011, **54**(10), 3451–3479.
37 J. F. Hartwig, Carbon–heteroatom bond-forming reductive eliminations of amines, ethers, and sulfides, *Acc. Chem. Res.*, 1998, **31**(12), 852–860.
38 C.-X. Yu, *et al.*, Selective MT2 melatonin receptor antagonist blocks melatonin-induced antinociception in rats, *Neurosci. Lett.*, 2000, **282**(3), 161–164.
39 L. Rajmohan and V. Mohan, Repaglinide: the prandial glucose regulator-a new class of oral antidiabetic drugs, *Proceedings of Scientific Sessions, APICON 2000*, 2000, vol. 10, pp. 519–521.
40 D. Ma and Q. Cai, Copper/amino acid catalyzed cross-couplings of aryl and vinyl halides with nucleophiles, *Acc. Chem. Res.*, 2008, **41**(11), 1450–1460.
41 F. Monnier and M. Taillefer, Catalytic C☐C, C☐N, and C☐O Ullmann-Type Coupling Reactions, *Angew. Chem., Int. Ed.*, 2009, **48**(38), 6954–6971.
42 D. S. Surry and S. L. Buchwald, Diamine ligands in copper-catalyzed reactions, *Chem. Sci.*, 2010, **1**(1), 13–31.
43 E. Olcay, *et al.*, Oral toxicity of pefloxacin, norfloxacin, ofloxacin and ciprofloxacin: comparison of biomechanical and histopathological effects on Achilles tendon in rats, *J. Toxicol. Sci.*, 2011, **36**(3), 339–345.
44 R. Iacovino, *et al.*, β-Cyclodextrin inclusion complex to improve physicochemical properties of pipemidic acid: Characterization and bioactivity evaluation, *Int. J. Mol. Sci.*, 2013, **14**(7), 13022–13041.
45 E. E. Kwan, *et al.*, Concerted nucleophilic aromatic substitutions, *Nat. Chem.*, 2018, **10**(9), 917–923.
46 C. Liu, *et al.*, Celecoxib alleviates nonalcoholic fatty liver disease by restoring autophagic flux, *Sci. Rep.*, 2018, **8**(1), 1–10.

47 S. M. Islam, *et al.*, Highly efficient recyclable polymer anchored palladium catalyst for CC and CN coupling reactions, *J. Mol. Catal. A: Chem.*, 2013, **366**, 321–332.
48 N. Esfandiary, S. Bagheri and A. Heydari, Magnetic γ-Fe_2O_3@ Cu-LDH intercalated with Palladium Cysteine: An efficient dual nano catalyst in tandem CN coupling and cyclization progress of synthesis quinolines, *Appl. Clay Sci.*, 2020, **198**, 105841.
49 M. A. Alavi, *et al.*, Ultrasound and modulation assisted synthesis of {[Cu_2(BDC-NH_2)$_2$(dabco)]·DMF·3H2O} nanostructures; New precursor to prepare nanorods and nanotubes of copper (II) oxide, *Ultrason. Sonochem.*, 2015, **22**, 349–358.
50 N. K. Gupta, *et al.*, Fabrication of Cu(BDC)$_{0.5}$(BDC-NH_2)$_{0.5}$ metal-organic framework for superior H_2S removal at room temperature, *Chem. Eng. J.*, 2021, **411**, 128536.
51 J. F. Kurisingal, *et al.*, Facile green synthesis of new copper-based metal–organic frameworks: Experimental and theoretical study of the CO_2 fixation reaction, *ACS Sustainable Chem. Eng.*, 2020, **8**(29), 10822–10832.
52 R. Kumar, *et al.*, Regioselective Mannich bases of pyrrole-2-carbaldehyde and binuclear copper (II) complexes of bis (iminopyrrolyl) ligand containing the piperazine ring, *Inorg. Chim. Acta*, 2016, **445**, 70–78.
53 D. A. Skoog, F. J. Holler and S. R. Crouch, *Instrumental analysis*, Brooks/Cole, Cengage Learning, Belmont, 2007, vol. 47.
54 C. A. Gorski and M. M. Scherer, Determination of nanoparticulate magnetite stoichiometry by Mossbauer spectroscopy, acidic dissolution, and powder X-ray diffraction: A critical review, *Am. Mineral.*, 2010, **95**(7), 1017–1026.
55 A. Coats and J. Redfern, Thermogravimetric analysis. A review, *Analyst*, 1963, **88**(1053), 906–924.
56 D. Stokes, *Principles and practice of variable pressure/environmental scanning electron microscopy (VP-ESEM)*, John Wiley & Sons, 2008.
57 L. Corbari, *et al.*, Iron oxide deposits associated with the ectosymbiotic bacteria in the hydrothermal vent shrimp Rimicaris exoculata, *Biogeosciences*, 2008, **5**(5), 1295–1310.
58 K. Ratkanthwar, *et al.*, Schlenk techniques for anionic polymerization, *Anionic Polymerization: Principles, Practice, Strength, Consequences and Applications*, 2015, pp. 3–18.
59 M. Sajjadi, M. Nasrollahzadeh and H. Ghafuri, Cu (II)-*N*-benzyl-amino-1*H*-tetrazole complex immobilized on magnetic chitosan as a highly effective nanocatalyst for CN coupling reactions, *J. Organomet. Chem.*, 2021, **950**, 121959.
60 Z. Khorsandi, *et al.*, Sustainable synthesis of potential antitumor new derivatives of Abemaciclib and Fedratinib *via* CN cross coupling reactions using Pd/Cu-free Co-catalyst, *Mol. Catal.*, 2022, **517**, 112011.
61 F. Panahi, *et al.*, Immobilized Pd nanoparticles on silica-starch substrate (PNP-SSS): Efficient heterogeneous catalyst in Buchwald–Hartwig C–N cross coupling reaction, *J. Organomet. Chem.*, 2017, **851**, 210–217.